Journal of Molecular Structure: THEOCHEM 910 (2009) 34–40

Contents lists available at ScienceDirect

Journal of Molecular Structure: THEOCHEM

journal homepage: www.elsevier.com/locate/theochem

Theoretical study of the reaction of CF_3O radicals with CO

Guohua Xu, Chengyin Shen, Haiyan Han, Jianquan Li, Hongmei Wang, Yannan Chu *

Laboratory of Environmental Spectroscopy, Anhui Institute of Optics and Fine Mechanism, Chinese Academy of Sciences, P.O. Box 1125, Hefei, 230031 Anhui, PR China

ARTICLE INFO

Article history:
Received 4 February 2009
Received in revised form 10 June 2009
Accepted 10 June 2009
Available online 18 June 2009

Keywords:
Radical reaction
Potential energy surface
Density functional theory
Ab initio calculation
Enthalpy of formation

ABSTRACT

The potential energy surface for the reaction of the CF_3O radicals with CO was investigated. The geometries and vibrational frequencies of the reactants, transition states, intermediates, and products were calculated at the UB3LYP/6-311+G(2d,p), UB3LYP/6-311+G(3df,2p) and UMP2/6-311+G(2d,p) levels of theory. The energies were improved by using the G2M(CC2) and G3B3 methods. The calculation suggests the reaction proceeds via either the fluorine abstraction of CF_3O by CO to produce FCO + CF_2O with a high energy barrier or the barrierless association of the reactants to form the *trans*-CF_3OCO intermediate. The *trans*-CF_3OCO is predicted to undergo subsequent isomerization to *cis*-CF_3OCO or dissociate directly to the products FCO + CF_2O and CF_3 + CO_2. The collisional stabilization of *trans*-CF_3OCO is dominant at room temperature, while *trans*-CF_3OCO isomerizing to *cis*-CF_3OCO followed by dissociating to CF_3 + CO_2 is accessible when temperature rises. The reason for only *trans*-CF_3OCO without *cis*-CF_3OCO observable in Ashen's experiment [S.V. Ahsen, J. Hufen, H. Willner, J.S. Francisco, Chem. Eur. J. 8 (2002) 1189] is *cis*-CF_3OCO can be produced only via the isomerization of *trans*-CF_3OCO, and its yield is inappreciable at a low experimental temperature. The enthalpies of formation for the two conformations of CF_3OCO have been deduced: $\Delta_f H^\circ_0$ (*trans*-CF_3OCO) = −196.25 kcal mol^{-1}, $\Delta_f H^\circ_{298.15}$ (*trans*-CF_3OCO) = −197.46 kcal mol^{-1}, $\Delta_f H^\circ_0$ (*cis*-CF_3OCO) = −193.64 kcal mol^{-1}, and $\Delta_f H^\circ_{298.15}$ (*cis*-CF_3OCO) = −194.90 kcal mol^{-1}.

1. Introduction

CF_3O radicals are generated in the atmosphere as a result of the oxidation of hydrofluorocarbons such as CHF_3, CF_3CH_2F and CF_3CHF_2 [1–9]. In view of their high reactivity against hydrocarbons [10–12], the reactions of CF_3O with the atmospheric trace constituents NO, NO_2 [13] and CO [14–19] have aroused intense interest. Among them the reaction between CF_3O and CO is a non-negligible sink for CF_3O in the atmosphere [14] by the following three possible exothermic channels:

$$CF_3O + CO + M \rightarrow CF_3OCO + M \quad (1a)$$

$$CF_3O + CO \rightarrow CF_3 + CO_2 \quad \Delta H^\circ_{298.15} = -22.34 \text{ kcal mol}^{-1} \quad (1b)$$

$$\rightarrow FCO + CF_2O \quad \Delta H^\circ_{298.15} = -10.58 \text{ kcal mol}^{-1} \quad (1c)$$

In the above reactions, the $\Delta H^\circ_{298.15}$ values for reactions (1b) and (1c) were calculated according to the formation enthalpies of the reactants and products [20,21]. Due to lack of the formation enthalpy of CF_3OCO, the $\Delta H^\circ_{298.15}$ value for channel (1a) is unknown.

Over the past decades, the reaction of CF_3O radical with CO has been studied by means of various experimental methods, and these experiments focused on the reaction rate measurement and the reaction products investigation. For instance, Czarnowski and Schumacher [15] studied this reaction over 315–343 K and in the pressure range of 100–500 Torr. They suggested that the reaction proceeds via an addition mechanism to give CF_3OCO. Zellner [16] reported the rate constant at 298 K for the title reaction in 66 Torr He gas to be 4.4×10^{-14} cm^3 molecule^{-1} s^{-1}, but they did not give any information about the reaction products. Turnipseed et al. [14] studied the CF_3O + CO reaction using the pulsed laser photolysis/pulsed laser induced fluorescence (PLP/PLIF) and discharge flow/chemical ionization mass spectrometry (DF/CIMS). Their PLP/PLIF measurements gave the rate constants over 233–332 K in the Arrhenius form $k = (2.0 \pm 0.6) \times 10^{-13}\exp[-(320 \pm 100)/T]$ cm^3 molecule^{-1} s^{-1}, which were considered as the high pressure limiting of the rate constants. The DF/CIMS experiments were also performed in a lower pressure range of 0.79–6.25 Torr, unfortunately no explicit products were detectable. According to the rate constant dependence on pressure, the authors considered channel (1a) to be the most feasible and reactions (1b) and (1c) to be minor at 298 K. Wallington and Ball [17] employed a relative rate technique to study the reaction of CF_3O with ^{13}CO at 296 K. The rate constants of the CF_3O + ^{13}CO reaction in 100 and 700 Torr air were measured to be $(4.6 \pm 0.5) \times 10^{-14}$ and $(7.2 \pm 0.7) \times 10^{-14}$ cm^3 molecule^{-1} s^{-1}, respectively. They speculated that the predominant product is CF_3OCO radical yielded via reaction (1a) at ambient condition; the channel (1c) to form FCO + CF_2O is petit, whereas the reaction (1b) to form CF_3 + CO_2 could not be excluded.

* Corresponding author. Address: Laboratory of Environmental Spectroscopy, Anhui Institute of Optics and Fine Mechanism, Chinese Academy of Sciences, 350 Shushan hu Road, P.O. Box 1125, Hefei, 230031 Anhui, PR China. Tel.: +86 551 5591076; fax: +86 551 5591572.
E-mail address: ychu@aiofm.ac.cn (Y. Chu).

0166-1280/$ - see front matter © 2009 Elsevier B.V. All rights reserved.
doi:10.1016/j.theochem.2009.06.012

In Meller's experiment [18], the CF_3O radicals were produced by photolyzing $CF_3O_2CF_3$ in the presence of CO in a static reactor kept at 296 K and with 760 Torr N_2 or air. The CF_3O + CO reaction rate was measured to be $(5.0 \pm 0.9) \times 10^{-14}$ cm^3 $molecule^{-1}$ s^{-1}. Since the infrared spectrum was observed from $CF_3OC(O)C(O)OCF_3$, a compound formed by the combination of two CF_3OCO radicals, the CF_3OCO is thought to be the main product through reaction (1a). However, the spectral observations did not find the products from reactions (1b) and (1c). Ahsen et al. [19] prepared CF_3O radicals from flash pyrolysis of $CF_3OC(O)OOCF_3$ or $CF_3OC(O)OOC(O)OCF_3$ in a high excess CO. By comparing with the calculated infrared spectra, the product CF_3OCO, formed through the route (1a), was identified to be in the form of *trans*-conformation.

As mentioned above, different experiments were carried out to identify the products of the CF_3O + CO reaction, however, no study is reported to theoretically elucidate the possibility of reactions (1a)–(1c). Moreover, one wonders why only *trans*-CF_3OCO without *cis*-CF_3OCO was observed in Ahsen's experiment. The aim of this study is to reveal the mechanism of the title reaction and to explore the reasons for the absence of *cis*-CF_3OCO in the experiments by density functional theory as well as *ab initio* calculation method. In addition, the enthalpies of formation are estimated for *trans*-CF_3OCO and *cis*-CF_3OCO. It is expected that this study would shed further light on the experiments.

2. Computational methods

All calculations were performed with the Gaussian03 program packages [22]. Geometries of minima and transition states on the doublet potential energy surface were optimized by using the density functional theory (DFT) UB3LYP method in conjunction with the 6-311+G(2d,p) and 6-311+G(3df,2p) basis sets, and the unrestricted Møller–Plesset second-order perturbation UMP2 method with the 6-311+G(2d,p) basis set. Vibrational frequencies at the same levels of theory were used to characterize stationary points and provide zero-point energies. The reactants, products and intermediates have all real frequencies, whereas every transition state possesses only one imaginary frequency. To confirm that a transition state connects the right reactants and products, the intrinsic reaction coordinate (IRC) path was calculated at the UB3LYP/6-311+G(3df,2p) level of theory. Single-point energy computations were performed by using the G2M(CC2) [23] and G3B3 [24] methods to improve the accuracy of energies.

3. Results and discussion

The optimized geometries of various species involved in the title reaction are shown in Fig. 1, and their vibrational frequencies are collected in Table 1 together with some available experimental values. Table 2 lists the energies of various stationary points relative to the reactants. Fig. 2 is the potential energy surface labeled with the energies of all species obtained at the G2M(CC2) and G3B3 levels.

3.1. Assessment of the computational methods

Since UHF wave functions are not spin eigenfunctions, the expectation values of $\langle S^2 \rangle$ were monitored to check the spin contamination. For doublets, $\langle S^2 \rangle$ was found to be in the range of 0.751–0.767 at the UB3LYP/6-311+G(2d,p) and UB3LYP/6-311+G(3df,2p) levels, which is somewhat beyond its exact value of 0.750. In contrast, at the UMP2/6-311+G(2d,p) level, $\langle S^2 \rangle$

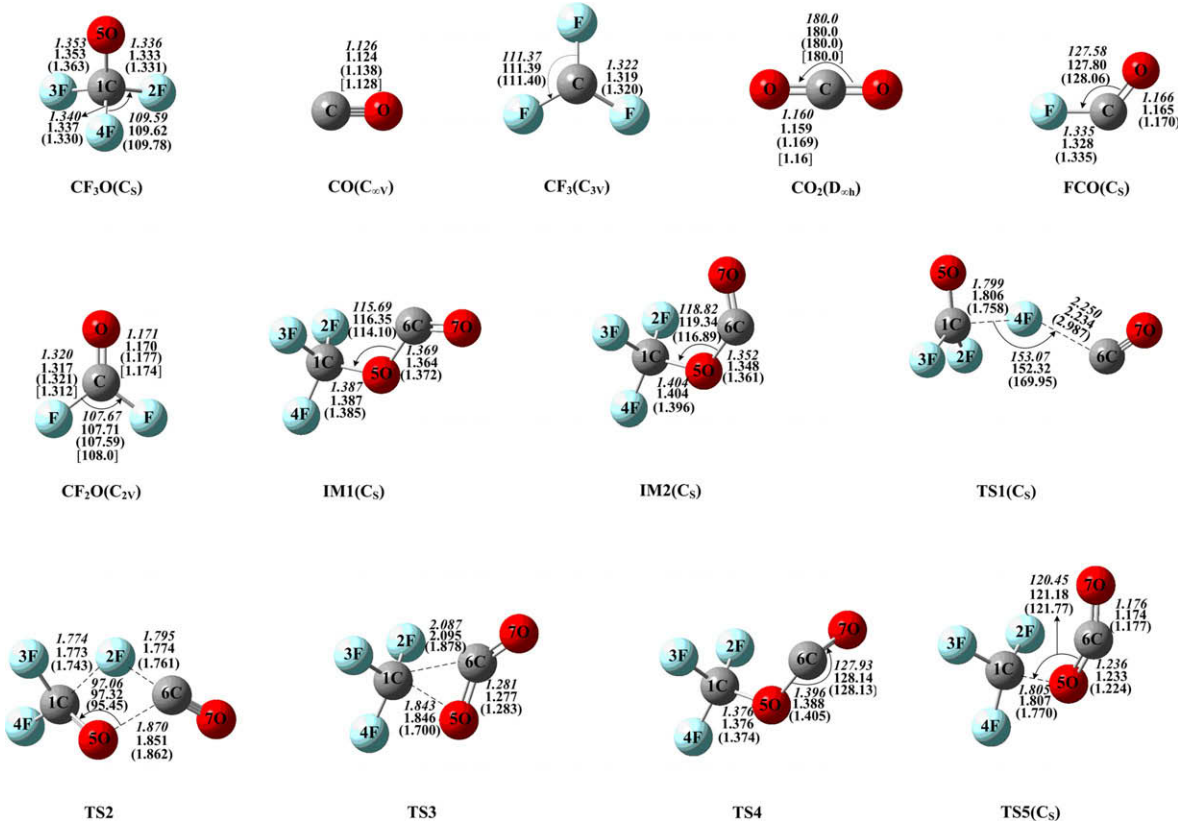

Fig. 1. The optimized geometries of the reactants, transition states and products for the CF_3O + CO reaction. Bond lengths in angstrom and bond angles in degree. Numbers in italics, roman and parenthesis show the results calculated at the UB3LYP/6-311+G(2d,p), UB3LYP/6-311+G(3df,2p) and UMP2/6-311+G(2d,p) levels of theory respectively. Numbers in square brackets are available experimental values.

Table 1
Vibrational frequencies (cm^{-1}) for stationary points on the potential energy surface of the $CF_3O + CO$ reaction along with available experimental values.

Species	Methods	Frequencies															
CF_3O	UB3LYP/6-311+G(2d,p)	260	399	567	585	607	883	1130	1174	1234							
	UB3LYP/6-311+G(3df,2p)	264	401	572	591	613	891	1144	1185	1241							
	UMP2/6-311+G(2d,p)	241	418	585	600	623	896	1219	1229	1289							
	Exp[a]			622		663	894	1199	1207	1260							
CO	UB3LYP/6-311+G(2d,p)	2211															
	UB3LYP/6-311+G(3df,2p)	2217															
	UMP2/6-311+G(2d,p)	2114															
	Exp[b]	2169.52															
IM1	UB3LYP/6-311+G(2d,p)	91	191	193	414	423	469	605	606	715	896	1017	1176	1200	1254	1915	
	UB3LYP/6-311+G(3df,2p)	90	192	194	416	427	472	610	613	722	904	1034	1180	1214	1265	1924	
	UMP2/6-311+G(2d,p)	98	195	202	421	433	477	615	619	723	908	1050	1214	1239	1292	1899	
	Exp[c]				418		475	612	612	720	902	997	1203	1236	1280	1857	
IM2	UB3LYP/6-311+G(2d,p)	74	176	264	369	439	549	575	608	805	838	1022	1133	1213	1252	1880	
	UB3LYP/6-311+G(3df,2p)	76	176	266	372	443	554	579	614	809	844	1034	1142	1226	1264	1889	
	UMP2/6-311+G(2d,p)	89	184	269	377	449	558	590	622	810	852	1075	1167	1248	1291	1869	
TS1	UB3LYP/6-311+G(2d,p)	577i	18	49	67	94	196	252	309	577	586	592	938	1243	1580	2213	
	UB3LYP/6-311+G(3df,2p)	570i	16	51	66	95	200	253	308	582	593	597	950	1256	1601	2218	
	UMP2/6-311+G(2d,p)	1186i	15	16	32	34	75	262	356	604	616	660	998	1299	1622	2113	
TS2	UB3LYP/6-311+G(2d,p)	583i	58	205	265	289	380	465	540	593	603	746	958	1267	1524	2072	
	UB3LYP/6-311+G(3df,2p)	582i	59	211	269	292	385	474	549	600	608	754	969	1283	1540	2067	
	UMP2/6-311+G(2d,p)	540i	54	242	286	307	409	486	583	608	625	772	963	1279	1568	2037	
TS3	UB3LYP/6-311+G(2d,p)	896i	18	167	181	331	409	501	556	683	706	946	1098	1237	1247	1955	
	UB3LYP/6-311+G(3df,2p)	906i	23	166	184	332	408	506	561	689	711	955	1109	1252	1264	1967	
	UMP2/6-311+G(2d,p)	1108i	48	211	291	432	491	538	580	738	758	918	1069	1226	1326	1983	
TS4	UB3LYP/6-311+G(2d,p)	203i	55	207	374	416	535	589	631	700	821	984	1147	1172	1241	1913	
	UB3LYP/6-311+G(3df,2p)	207i	54	203	377	419	540	595	636	705	833	1003	1152	1185	1253	1919	
	UMP2/6-311+G(2d,p)	216i	62	209	381	426	545	603	643	707	833	992	1188	1212	1285	2127	
TS5	UB3LYP/6-311+G(2d,p)	669i	32	122	209	254	503	517	550	567	742	983	1120	1264	1282	2019	
	UB3LYP/6-311+G(3df,2p)	662i	30	121	212	256	508	522	555	573	746	994	1129	1280	1298	2035	
	UMP2/6-311+G(2d,p)	1752i	23	112	220	257	518	523	536	617	768	977	1112	1280	1303	2058	
CF_2O	UB3LYP/6-311+G(2d,p)	574	614	777	956	1207	1959										
	UB3LYP/6-311+G(3df,2p)	578	617	780	967	1221	1966										
	UMP2/6-311+G(2d,p)	584	620	782	955	1225	1939										
	Exp[d]	584	626	774	965	1249	1928										
FCO	UB3LYP/6-311+G(2d,p)	625	1011	1915													
	UB3LYP/6-311+G(3df,2p)	632	1035	1923													
	UMP2/6-311+G(2d,p)	632	1039	1957													
	Exp[e]	626	1018	1855													
CF_3	UB3LYP/6-311+G(2d,p)	500	500	690	1064	1220	1220										
	UB3LYP/6-311+G(3df,2p)	504	504	698	1076	1235	1235										
	UMP2/6-311+G(2d,p)	511	511	705	1099	1256	1256										
	Exp[f]	500	500	701	1090	1259	1259										
CO_2	UB3LYP/6-311+G(2d,p)	676	676	1364	2400												
	UB3LYP/6-311+G(3df,2p)	679	679	1374	2414												
	UMP2/6-311+G(2d,p)	663	663	1317	2398												
	Exp[g]	667.30	667.30	1384.86	2349.30												

[a] Ref. [34], in Ar-matrix.
[b] Ref. [25].
[c] Ref. [19].
[d] Ref. [35].
[e] Ref. [36].
[f] Ref. [37,38].
[g] Ref. [26].

changes in the range of 0.754–0.880. Thus, spin contamination is ignorable for UB3LYP method, but severe in the UMP2 computation.

In all species listed in Fig. 1, the experimental geometry parameters are available only for CO, CO_2 and CF_2O. The experimental bond length of CO is 1.128 Å [25], and the theoretical values are 1.126, 1.124 and 1.138 Å, respectively, at the UB3LYP/6-311+G(2d,p), UB3LYP/6-311+G(3df,2p) and UMP2/6-311+G(2d,p) levels. The C–O bond length in CO_2 is 1.160 Å according to the experimental result [26], and the calculation values are 1.160, 1.159 and 1.169 Å, respectively, at the UB3LYP/6-311+G(2d,p), UB3LYP/6-311+G(3df,2p) and UMP2/6-311+G(2d,p) levels. One can note that the UB3LYP method are superior to the UMP2, and the UB3LYP/6-311+G(2d,p) calculation gives better prediction for the structures of CO and CO_2 than the UB3LYP/6-311+G(3df,2p) level of theory.

For CF_2O, the experimental values of the C–F bond length and the FCF angle are 1.312 Å and 108.0°, respectively [27]. The UB3LYP/6-311+G(2d,p) method predicts a C–F bond of 1.320 Å and a FCF angle of 107.67°, while the UB3LYP/6-311+G(3df,2p) calculation results in a C–F bond length of 1.317 Å and a FCF angle of 107.71°. Thus, the UB3LYP/6-311+G(3df,2p) level can produce much better results for the C–F bond and the FCF angle in CF_2O. Considering the vibrational frequencies (Table 1) are also well

Table 2
Energies (kcal mol^{-1}) of products, intermediates, and transition states relative the CF_3O + CO reactants.

Species	UB3LYP/6-311+G(3df,2p)	G2(MCC2)	G3B3
CF_3O + CO	0.0	0.0	0.0
FCO + CF_2O	−15.29	−8.98	−10.26
CF_3 + CO_2	−34.40	−27.71	−29.31
IM1	−19.42	−18.20	−18.85
IM2	−16.44	−15.65	−16.23
TS1	22.15	32.38	32.83
TS2	23.07	30.36	28.63
TS3	27.43	34.71	33.14
TS4	−11.50	−10.62	−11.41
TS5	−2.61	6.89	5.56

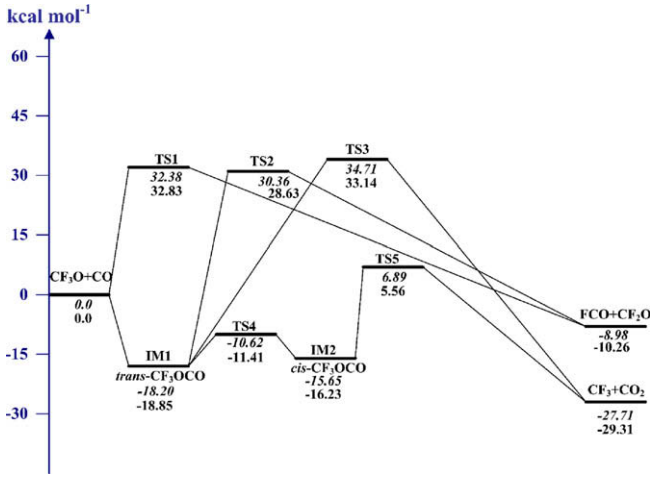

Fig. 2. The doublet potential energy surface (PES) for the CF_3O + CO reaction. The relative energies at G2M(CC2) and G3B3 levels of theory are shown in the italics and roman type respectively.

predicted at the UB3LYP/6-311+G(3df,2p) level for the species whose experimental values are available, in the following mechanism study we adopt the structural parameters and vibrational frequencies obtained at the UB3LYP/6-311+G(3df,2p) level of theory.

3.2. Direct abstraction mechanism

As shown in Figs. 1 and 2, the C atom of CO may abstract the F atom of CF_3O to form the products FCO + CF_2O via the transition state TS1. The barrier heights of TS1 are estimated to be 32.38 and 32.83 kcal mol^{-1} at G2M(CC2) and G3B3 levels, respectively. In TS1, the breaking 1C–4F bond is stretched to 1.806 Å, which is 0.469 Å longer than the 1C—4F bond in parent CF_3O. The forming 6C–4F bond has a length of 2.234 Å, and it is 0.906 Å longer than the C–F bond of the product FCO. The transition state TS1 has a Cs symmetry and is a first-order saddle point with an imaginary frequency of 570i cm^{-1} (Table 1). As shown in Table 2 and Fig. 2, the F atom abstraction reaction of CF_3O by CO is exothermic. The reaction enthalpies at 0 K for the products FCO + CF_2O are −8.98 and −10.26 kcal mol^{-1}, respectively, at the G2M(CC2) and G3B3 levels. The counterparts at 298.15 K are −9.14 and −10.43 kcal mol^{-1}. The predicted reaction enthalpy of −10.43 kcal mol^{-1} at the G3B3 level is very close to an experimental value of −10.58 kcal mol^{-1} [20,21].

3.3. Addition–elimination mechanism

3.3.1. Initial association

The O atom of CF_3O radical has an unpaired electron, and it may add firstly to either C or O atom of CO. It can be verified that the C site in CO would be more favorable by the Fukui function analysis. For a molecular system, the Fukui function [28] is defined as $f(\vec{r}) = [\partial\rho(\vec{r})/\partial N]_\upsilon$. The $f(\vec{r})$ characterizes the sensitivity of electron density $\rho(\vec{r})$ to a change in electron number N at constant external potential υ. It is well-known that, the greater the Fukui function value, the greater the reactivity of a site [28]. Normally, the Fukui function has three different forms, $f^+(\vec{r})$, $f^-(\vec{r})$ and $f^0(\vec{r})$ [28], which govern nucleophilic, electrophilic and radical attacks, respectively. Yang and Mortier [29] proposed a condensed-to-atom form of the Fukui function, where the condensed Fukui functions of the atom, k, in a molecule with N electrons are expressed as

$$f_k^+ = q_k(N+1) - q_k(N) \quad \text{for nucleophilic attack}$$
$$f_k^- = q_k(N) - q_k(N-1) \quad \text{for electrophilic attack}$$
$$f_k^0 = 1/2[q_k(N+1) - q_k(N-1)] \quad \text{for radical attack}$$

where $q_k(N+1)$, $q_k(N)$ and $q_k(N-1)$ are the electronic populations of atom k in the systems with $N+1$, N and $N-1$ electrons, respectively.

Since the CF_3O approaching CO is a radical attack, we choose f_k^0 to describe the reactivity of the carbon and oxygen atoms in CO. In the present work, the electronic populations were evaluated by natural population analysis (NPA). The f_k^0 values of C atom in CO are 0.792 and 0.795 at the UB3LYP/6-311+G(2d,p) and UB3LYP/6-311+G(3df,2p) levels, respectively, whereas the f_k^0 values of O atom are 0.208 and 0.205, respectively, at the same levels of theory. The f_k^0 value of C atom is much larger than that of O atom, thus the C atom in CO will be more easily attacked by the O atom of CF_3O radical.

When CF_3O attacks CO, the O atom of CF_3O can approach the C atom of CO in *trans*-manner or *cis*-manner. The former would lead to the formation of *trans*-CF_3OCO intermediate (IM1) whose dihedral angle τ(7O,6C,5O,1C) is −180°. The latter is expected to produce *cis*-CF_3OCO intermediate (IM2), whose dihedral angle τ(7O,6C,5O,1C) is 0°.

Fig. 3 shows the relaxed potential energy curves for *trans*-CF_3O-CO and *cis*-CF_3OCO calculated at the UB3LYP/6-311+G(3df,2p) level using the 5O–6C bond as the scanned coordinate. It can be found that the potential energy curve to form *trans*-CF_3OCO is barrierless, whereas the curve connecting *cis*-CF_3OCO with the reactants is discontinuous at r(5O–6C) = 1.925 Å. For illuminating the reason for this phenomena, a relaxed potential energy surface scan using both the 5O–6C bond and the dihedral angle τ(7O,6C,5O,1C) as scanned coordinates will be needed. Since such a potential energy surface

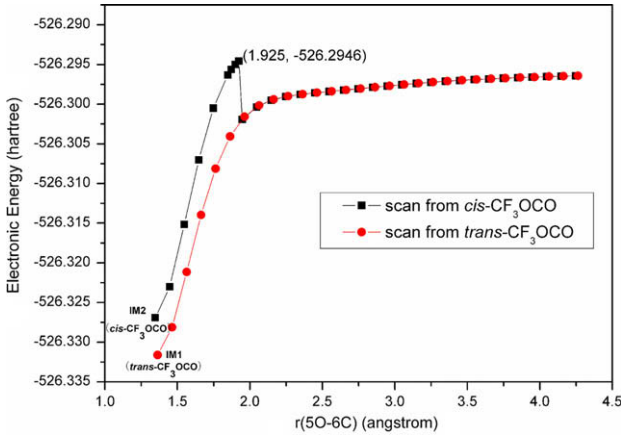

Fig. 3. Relaxed potential energy surface scan for the association reaction of CF_3O with CO using the 5O–6C bond as scanned coordinate at UB3LYP/6-311+G(3df,2p) level of theory (●) Scan starting from *trans*-CF_3OCO (■) Scan starting from *cis*-CF_3OCO.

scan is computationally expensive, a two-dimensional rigid potential energy surface scan at the UB3LYP/6-311+G(3df,2p) level was performed to give a qualitative explanation.

In the two-dimensional rigid potential energy surface scan, the varied coordinates are the 5O–6C bond and the dihedral angle τ(7O,6C,5O,1C). The increment of the 5O–6C bond is 0.075 Å in the range of 1.2725–2.1725 Å, and 0.15 Å from 2.1725 to 3.0725 Å, while the step size of dihedral angle τ(7O,6C,5O,1C) is 15° over a range from −210° to 60°. The other geometrical parameters are fixed at the optimized values of *cis*-CF_3OCO at UB3LYP/6-311+G(3df,2p) level of theory. The resulting rigid potential energy surface is shown in Fig. 4(a), in which A point at r(5O–6C) = 1.3475 Å and τ(7O,6C,5O,1C) = −180°, and B point at r(5O–6C) = 1.3475 Å and τ(7O,6C,5O,1C) = 0° correspond to *trans*-CF_3OCO and *cis*-CF_3OCO, respectively.

Fig. 4(b) represents the energy variation versus τ(7O,6C,5O,1C) at the five fixed r(5O–6C) values. At a small r(5O–6C), the curves have two minima located at τ(7O,6C,5O,1C) = 0° and −180°, respectively. However, when r(5O–6C) increases to a specific value between 1.7975 Å (D point) and 1.8725 Å (E point), the minimum at τ(7O,6C,5O,1C) = 0° changes into a maximum, while the potential well at τ(7O,6C,5O,1C) = −180° becomes shallow. Thus, if one uses r(5O–6C) as the unique scanned coordinate and starts the scan from the equilibrium geometry of *cis*-CF_3OCO, the optimized geometry would converge to the structure with τ(7O,6C,5O,1C) = 0° provided that r(5O–6C) is less than the specific value between 1.7975 and 1.8725 Å, but would go to the lower energy structure with τ(7O,6C,5O,1C) = −180° once r(5O–6C) exceeds this specific value. This shows that the relaxed potential energy curve starting from *cis*-CF_3OCO actually converges to the potential energy curve scanning from *tans*-CF_3OCO when r(5O–6C) increases over the specific value, thereby resulting in a discontinuity as shown in Fig. 3.

In Fig. 4(a) and (b), the r(5O–6C) value for the discontinuity on the relaxed potential energy curve should be between 1.7975 and 1.8725 Å. However, Fig. 3 shows that the discontinuity locates at r(5O–6C) = 1.925 Å. This discrepancy may be owing to the approximate treatment using the rigid scan instead of the relaxed scan.

In fact, the discontinuity of the relaxed potential energy curve is due to the existence of a second-order saddle point between the reactants and *cis*-CF_3OCO. This second-order saddle point is represented by the F point in Fig. 4(a) at r(5O–6C) = 2.0975 Å and τ(7O,6C,5O,1C) = 0°. At the UB3LYP/6-311+G(3df,2p) level of theory, a fully optimization leads to r(5O–6C) = 2.0622 at the second-order saddle point, which is consistent with the 5O–6C bond length of 2.0975 Å of F point. The second-order saddle point prevents the $CF_3O + CO$ reaction from directly forming *cis*-CF_3OCO. Thus, in the potential energy surface (Fig. 2), we do not connect the reactants with *cis*-CF_3OCO.

3.3.2. Isomerization and dissociation

trans-CF_3OCO lies −18.20 and −18.85 kcal mol^{-1} below the reactants at the G2M(CC2) and G3B3 levels, respectively, and the reaction enthalpy at 298.15 K for *trans*-CF_3OCO formation is −19.06 and −19.67 kcal mol^{-1}, respectively, at the same levels. As shown in Fig. 2, there are three primary pathways following the *trans*-CF_3OCO intermediate IM1. The first is the decomposition to the products $FCO + CF_2O$. This process may take place via a four-center transition state TS2 that results from the cleavage of the 1C–2F and 6C–5O bonds, and the formation of the 6C–2F bond. The broken 1C–2F and 5O–6C bond lengths in TS2 increase to 1.773 and 1.851 Å, respectively, the forming 2F–6C bond length decreases to 1.774 Å. The relevant energy barriers are 48.56 and 47.48 kcal mol^{-1}, respectively, by using the G2M(CC2) and G3B3 methods.

The second pathway involves the rupture of the 1C–5O bond through the transition state TS3, leading directly to the products $CF_3 + CO_2$. The 1C–5O bond undergoes substantial elongation by 0.459 Å compared with that in *trans*-CF_3OCO. The calculated imaginary frequency of 906i cm^{-1} characterizes this structure as a first-order saddle point, and the corresponding energy barrier is 52.91 and 51.99 kcal mol^{-1}, respectively, at the G2M(CC2) and G3B3 levels of theory. Fig. 5 shows the intrinsic reaction coordinate (IRC) scan curve of TS3 and the geometrical parameter changes along the reaction coordinate. It can be found that r(1C–5O), r(1C–6C) and 5O–6C–7O angle all increase along the route from *trans*-CF_3OCO to $CF_3 + CO_2$. The gradually increase of 5O–6C–7O angle to almost 180° brings the 5O–6C–7O moiety to approach the linear configuration of CO_2. This process is comparable to an analogous reaction *trans*-$CH_3OCO \rightarrow CH_3 + CO_2$ as reported by Francisco [30].

Another reaction channel proceeds first by an isomerization of *trans*-CF_3OCO via transition state TS4 to *cis*-CF_3OCO, which is

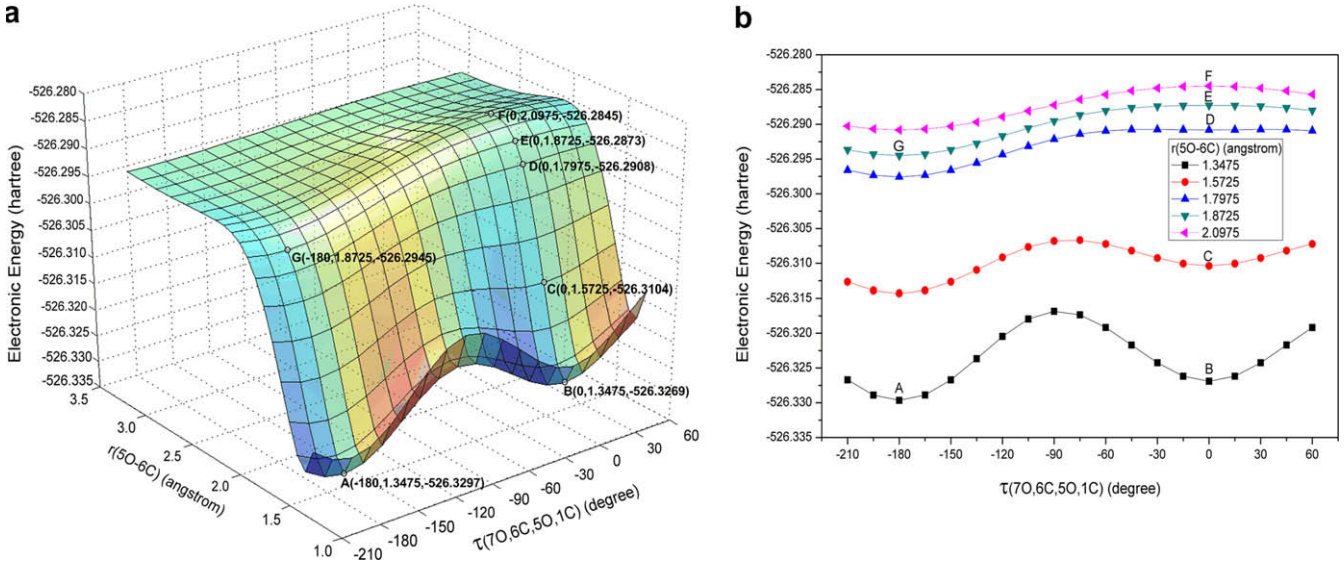

Fig. 4. (a) Potential energy surface for the association reaction of CF_3O with CO obtained by two-dimensional rigid scan at UB3LYP/6-311+G(3df,2p) level of theory. The scanned coordinates are the 5O–6C bond and the dihedral angle τ(7O,6C,5O,1C). (b) Potential energy curves representing the energy variation versus τ(7O,6C,5O,1C) at fixed r(5O–6C) values: (■) 1.3475 Å, (●) 1.5725 Å, (▲) 1.7975 Å, (▼) 1.8725 Å, and (◀) 2.0975 Å.

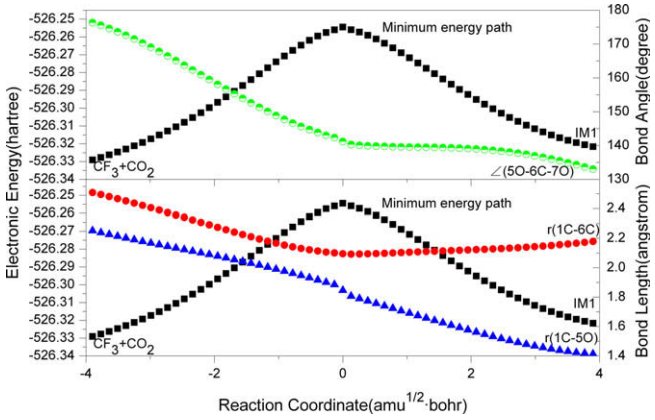

Fig. 5. The intrinsic reaction coordinate scan curve and changes of the relevant geometrical parameters along the reaction coordinate of transition state TS3.

2.55 and 2.62 kcal mol^{-1} higher in energy than *trans*-CF_3OCO at the G2M(CC2) and G3B3 levels, respectively. The isomerization energy barriers are 7.58 and 7.44 kcal mol^{-1}, respectively, at the G2M(CC2) and G3B3 levels of theory. *cis*-CF_3OCO further decomposes to the products $CF_3 + CO_2$ through the transition state TS5. The breaking 1C–5O bond in TS5 is elongated to 1.807 Å, which is 0.403 Å longer than that in *cis*-CF_3OCO. The barrier heights of TS5 are estimated to be 22.54 and 21.79 kcal mol^{-1}, respectively, at the G2M(CC2) and G3B3 levels of theory. And TS5 locates 6.89 and 5.56 kcal mol^{-1} above the reactants at the same levels. Compared with other reaction pathways aforementioned, this pathway has lower energy barriers at the transition states TS4 and TS5, and it should be available in the case of high experimental temperature.

3.4. The formation enthalpy of CF_3OCO

Though the CF_3OCO radicals were observed by Ahsen et al. [19] and confirmed as the main product of the reaction between CF_3O and CO at room temperature [18]. As far as we know, neither experimental nor theoretical data was reported about the formation enthalpy of CF_3OCO. In this work, the formation enthalpies of CF_3OCO are estimated by using the atomization reaction method [31,32].

The formation enthalpy of molecule M at 0 K is given by

$$\Delta_f H_0^\circ(M) = \sum_i^{\text{atoms}} \Delta_f H_0^\circ(X_i) - \sum D_0 \quad (2a)$$

where $\Delta_f H_0^\circ(X_i)$ is the experimental formation enthalpy of the isolated atom X_i [20], and ΣD_0 is the calculated atomization energy of the molecule M. In addition, the enthalpies of formation at 298.15 K can also be computed according the following equation.

$$\Delta_f H_{298.15}^\circ(M) = \Delta_f H_0^\circ(M) + [H_{298.15}^\circ(M) - H_0^\circ(M)] - \sum_i^{\text{atoms}} [H_{298.15}^\circ(X_i) - H_0^\circ(X_i)]_{\text{ref}} \quad (2b)$$

where $[H_{298.15}^\circ(M) - H_0^\circ(M)]$ is the calculated heat capacity correction for the molecule [31], and $[H_{298.15}^\circ(X_i) - H_0^\circ(X_i)]_{\text{ref}}$ is the heat capacity correction for the reference state of the atom X_i [20], which is 0.25, 1.04 and 1.05 kcal mol^{-1} for carbon , oxygen and fluorine atom, respectively.

The formation enthalpies of *trans*-CF_3OCO are deduced to be $\Delta_f H_0^\circ = -201.60$ and $\Delta_f H_{298.15}^\circ = -202.91$ kcal mol^{-1} at the G2M(CC2) level, and $\Delta_f H_0^\circ = -196.25$ and $\Delta_f H_{298.15}^\circ = -197.46$ kcal mol^{-1} at the G3B3 level. For *cis*-CF_3OCO, the formation enthalpies are $\Delta_f H_0^\circ = -199.06$ and $\Delta_f H_{298.15}^\circ = -200.42$ kcal mol^{-1} at the G2M(CC2) level, while $\Delta_f H_0^\circ = -193.64$ and $\Delta_f H_{298.15}^\circ = -194.90$ kcal mol^{-1} at the G3B3 level. Since the average deviation in the formation enthalpies was found to be 1.65 kcal mol^{-1} when using the G3B3 method [24], whereas no deviation data was reported for the G2M(CC2) method, the formation enthalpies calculated at G3B3 level of theory are more reliable.

3.5. Comparison with experiments

In Turnipseed's DF/CIMS experiments about the CF_3O + CO reaction [14], to determine the product CF_3, they added excess O_2 so as to convert CF_3 to CF_3O_2, whose anion $CF_3O_2^-$ can be formed by the charge transfer reaction with SF_6^-. However, the addition of excess O_2 did not produce the $CF_3O_2^-$ signal. The second method to detect CF_3 was carried out by using the charge transfer reaction of CF_3 with O_2^- to produce CF_3^-, but there were no CF_3^- signals detectable yet. In the FCO product investigation, Turnipseed et al. observed an ion signal at $m/z = 98$ when excess O_2 was added to the CF_3O + CO system. They speculated that the ions at $m/ez = 98$ correspond to $F_2CO_3^-$, which may be an indication of the FCO production. However, this presumption was no confirmed.

According to the potential energy surface in Fig. 2, the products $CF_3 + CO_2$ can yield via two pathways through *trans*-CF_3OCO, in which the pathway $CF_3O + CO \rightarrow$ *trans*-$CF_3OCO \rightarrow$ TS4 $\rightarrow$ *cis*-$CF_3OCO \rightarrow$ TS5 $\rightarrow CF_3 + CO_2$ would occur at a high temperature because TS5 lies only 6.89 and 5.56 kcal mol^{-1}, respectively, above the reactants at the G2M(CC2) and (G3B3) levels of theory, and the energy barrier of 22.54 and 21.79 kcal mol^{-1} at the same levels is moderate. In fact, Czarnowski and Schumacher [33] reported the evidence for CF_3 formation over 458–503 K, supporting the present calculation results. For the formation of FCO + CF_2O, it can proceed via either decomposition of *trans*-CF_3OCO or direct F atom abstraction of CF_3O by CO. However, the two pathways go through the transition states TS2 and TS1 which have rather high energy barriers of 47.48 and 32.83 kcal mol^{-1}, respectively, at the G3B3 level of theory, making the FCO + CF_2O products formation very difficult even at a comparative high temperature.

The rate constant dependence on pressure were also measured for the CF_3O + CO reaction [14,17], and the rate constant was found to increase with pressure at room temperature. This could be explained by the potential energy surface presented in this work. Due to the high energy barrier of TS1, the formation of FCO + CF_2O via direct fluorine abstraction reaction can be excluded first. The reaction has to start via the association of CF_3O with CO to form the *trans*-CF_3OCO intermediate. At room temperature, further decompositions of the *trans*-CF_3OCO intermediate are hindered by the high energy barriers of TS2, TS3 and TS5, thus the collisional stabilization of *trans*-CF_3OCO is dominant. When the pressure increases, the stabilization of *trans*-CF_3OCO by colliding with bath gas will be easier, thereby resulting in a larger rate constant.

As discussed in Section 3.3.1, the CF_3O + CO reaction cannot directly form *cis*-CF_3OCO due to the second-order saddle point between the reactants and *cis*-CF_3OCO. The sole path to produce *cis*-CF_3OCO is the isomerization of *trans*-CF_3OCO via the transition state TS4. The *cis*-CF_3OCO can dissociate to $CF_3 + CO_2$ through the transition state TS5. Because the energy barrier for *cis*-CF_3OCO decomposition is 21.79 kcal mol^{-1} at the G3B3 level of theory, which is much higher than the isomerization energy barriers of 7.44 kcal mol^{-1} from *trans*-CF_3OCO to *cis*-CF_3OCO and 4.82 kcal mol^{-1} in the reverse direction at the G3B3 level, the transformation between the two conformations is considered to be at equilibrium according to the equilibrium state approximation and the relative population of *cis*-CF_3OCO and *trans*-CF_3OCO can be estimated based on the following equation

$$K_{eq} = \frac{C_{cis}}{C_{trans}} = \frac{q_{cis}}{q_{trans}} e^{-\frac{\Delta E}{k_b T}} \quad (3)$$

where K_{eq} is the equilibrium constant, C and q are the molecular density and partition function for the two isomers of CF_3OCO, and ΔE is the energy difference between *cis*-CF_3OCO and *trans*-CF_3OCO, which is 2.62 kcal mol^{-1} at the G3B3 level of theory. T and k_b are temperature and Boltzmann constant respectively. In Ahsen's experiment [19], the matrix mixtures containing CF_3OCO were kept at 16 K during the experiments, and the proportion of *cis*-CF_3OCO relative to *trans*-CF_3OCO is only 1.40×10^{-36} according to Eq. (3). Thus *cis*-CF_3OCO could not be observed in Ahsen's experiment due to the extremely low temperature.

In Meller's experiment [18], the CF_3O radicals were produced by photolyzing $CF_3O_2CF_3$ in the presence of CO. The pressure of the static reactor was kept at 760 Torr, and the experimental temperature was 296 K. Under such circumstance, the proportion of *cis*-CF_3OCO relative to *trans*-CF_3OCO is estimated to be 0.01 by using Eq. (3). Therefore, for the bis-perfluoromethyl-oxalate $CF_3OC(O)C(O)OCF_3$ observed in the infrared spectrum, it is likely from the combination of two *trans*-CF_3OCO.

4. Conclusions

The mechanism of the $CF_3O + CO$ reaction was studied by density functional theory as well as *ab initio* method. Four reaction pathways were identified including the fluorine atom abstraction reaction and the association reaction followed by isomerization and decomposition.

$$CF_3O + CO \rightarrow TS1 \rightarrow FCO + CF_2O \quad (4a)$$

$$CF_3O + CO \rightarrow \textit{trans}\text{-}CF_3OCO \rightarrow TS2 \rightarrow FCO + CF_2O \quad (4b)$$

$$CF_3O + CO \rightarrow \textit{trans}\text{-}CF_3OCO \rightarrow TS3 \rightarrow CF_3 + CO_2 \quad (4c)$$

$$CF_3O + CO \rightarrow \textit{trans}\text{-}CF_3OCO \rightarrow TS4 \rightarrow \textit{cis}\text{-}CF_3OCO \rightarrow TS5 \rightarrow CF_3 + CO_2 \quad (4d)$$

The title reaction proceeds mainly via the barrierless association reaction between CF_3O and CO to form the intermediate *trans*-CF_3OCO which is experimentally accessible after collision stabilization. *cis*-CF_3OCO can only form via the isomerization of *trans*-CF_3OCO, and the low temperature result in much lower proportion of *cis*-CF_3OCO than *trans*-CF_3OCO.

The pathway (4d) can lead to the formation of $CF_3 + CO_2$ when temperature is enough high, whereas the reactions (4a)/(4b) and (4c) will be very difficult to yield the products $FCO + CF_2O$ and $CF_3 + CO_2$ even at a high temperature owing to quite high energy barriers of TS1, TS2 and TS3.

The formation enthalpies of *trans*-CF_3OCO were calculated to be $\Delta_f H^\circ_0 = -196.25$ and $\Delta_f H^\circ_{298.15} = -197.46$ kcal mol^{-1} at the G3B3 level of theory. For *cis*-CF_3OCO, the counterparts were -193.64 and -194.90 kcal mol^{-1}.

Acknowledgements

Partial financial support by the National Natural Science Found of China (20577049, 20707025) and the Natural Science Foundation of Anhui (070411026) are greatly acknowledged.

References

[1] O.J. Nielsen, T. Ellermann, J. Sehested, E. Bartkiewicz, T.J. Wallington, M.D. Hurley, Int. J. Chem. Kinet. 24 (1992) 1009.
[2] E.O. Edney, D.J. Driscoll, Int. J. Chem. Kinet. 24 (1992) 1067.
[3] J. Sehested, T. Ellermann, O.J. Nielsen, T.J. Wallington, M.D. Hurley, Int. J. Chem. Kinet. 25 (1993) 701.
[4] E.C. Tuazon, R. Atkinson, J. Atmos. Chem. 16 (1993) 301.
[5] E.C. Tuazon, R. Atkinson, J. Atmos. Chem. 17 (1993) 179.
[6] T.J. Wallington, M.D. Hurley, J.C. Ball, E.W. Kaiser, Environ. Sci. Technol. 26 (1992) 1318.
[7] F. Caralp, R. Lesclaux, A.M. Dognon, Chem. Phys. Lett. 129 (1986) 433.
[8] P.D. Lightfoot, R.A. Cox, J.N. Crowley, M. Destriau, G.D. Hayman, M.E. Jenkin, G.K. Moortgat, Atmos. Environ. A 26 (1992) 1805.
[9] T.J. Wallington, P. Dagaut, M.J. Kurylo, Chem. Rev. 92 (1992) 667.
[10] H. Saathoff, R. Zellner, Chem. Phys. Lett. 206 (1993) 349.
[11] S.B. Barone, A.A. Turnipseed, A.R. Ravishanankara, J. Phys. Chem. 98 (1994) 4602.
[12] C. Bourbon, C. Fittschen, J.P. Sawerysyn, P. Devolder, J. Phys. Chem. 99 (1995) 15102.
[13] C. Fockenberg, H. Somniz, G. Bednarek, R. Zellner, Ber. Bunsen. Phys. Chem. 101 (1997) 1411.
[14] A.A. Turnipseed, S.B. Barone, N.R. Jensen, D.R. Hanson, C.J. Howard, A.R. Ravishankara, J. Phys. Chem. 99 (1995) 6000.
[15] J. Czarnowski, H.J. Schumacher, Int. J. Chem. Kinet. 13 (1981) 639.
[16] H. Saathoff, R. Zellner, Presented at the 12th International Symposium on Gas Kinetics, July 1992, University of Reading.
[17] T.J. Wallington, J.C. Ball, J. Phys. Chem. 99 (1995) 3201.
[18] R. Meller, G.K. Moortgat, Int. J. Chem. Kinet. 29 (1996) 579.
[19] S.V. Ahsen, J. Hufen, H. Willner, J.S. Francisco, Chem. Eur. J. 8 (2002) 1189.
[20] M.W. Chase Jr., NIST-JANAF Thermochemical Tables, fourth ed., J. Phys. Chem. Ref. Data Monograph No. 9 NIST, Gaithersburg, 1998.
[21] R. Atkinson, D.L. Baulch, R.A. Cox, R.F. Hampson Jr., J.A. Kerr, M.J. Rossi, J. Troe, J. Phys. Chem. Ref. Data 29 (2000) 167.
[22] M.J. Frisch, G.W. Trucks, H.B. Schlegel, G.E. Scuseria, M.A. Robb, J.R. Cheeseman, V.G. Zakrzewski, J.A. Montgomery Jr., R.E. Stratmann, J.C. Burant, S. Dapprich, J.M. Millam, A.D. Daniels, K.N. Kudin, M.C. Strain, O. Farkas, J. Tomasi, V. Barone, M. Cossi, R. Cammi, B. Mennucci, C. Pomelli, C. Adamo, S. Clifford, J. Ochterski, G.A. Petersson, P.Y. Ayala, Q. Cui, K. Morokuma, D.K. Malick, A.D. Rabuck, K. Raghavachari, J.B. Foresman, J. Cioslowski, J.V. Ortiz, B.B. Stefanov, G. Liu, A. Liashenko, P. Piskorz, I. Komaromi, R. Gomperts, R.L. Martin, D.J. Fox, T. Keith, M.A. Al-Laham, C.Y. Peng, A. Nanayakkara, C. Gonzalez, M. Challacombe, P.M.W. Gill, B.G. Johnson, W. Chen, M.W. Wong, J.L. Andres, M. Head-Gordon, E.S. Replogle, J.A. Pople, Gaussian 03 (Revision B.05), Gaussian Inc., Pittsburgh, PA, 2003.
[23] M. Mebel, K. Morokuma, M.C. Lin, J. Chem. Phys. 103 (1995) 7414.
[24] A.G. Baboul, L.A. Curtiss, P.C. Redfern, K. Raghavachari, J. Chem. Phys. 110 (1999) 7650.
[25] G. Herzberg, Molecular Spectra and Molecular Structure. I. Spectra of Diatomic Molecules, D. Van Nostrand Company Inc., New York, 1950.
[26] G. Herzberg, Molecular Spectra and Molecular Structure. II. Infrared and Raman Spectra, D. Van Nostrand Company Inc., New York, 1945.
[27] V.W. Laurie, D.T. Pence, R.H. Jackson, J. Chem. Phys. 37 (1962) 2995.
[28] R.G. Parr, W. Yang, J. Am. Chem. Soc. 106 (1984) 4049.
[29] W. Yang, W.J. Mortier, J. Am. Chem. Soc. 108 (1986) 5708.
[30] J.S. Francisco, Chem. Phys. 237 (1998) 1.
[31] L.A. Curtiss, K. Raghavachari, P.C. Redfern, J.A. Pople, J. Chem. Phys. 106 (1997) 1063.
[32] R. Asatryan, J.W. Bozzelli, J.M. Simmie, J. Phys. Chem. A 112 (2008) 3172.
[33] J. Czarnowski, H.J. Schumacher, Z. Phys. Chem. Neue Fol. 92 (1974) 329.
[34] G.A. Arguello, H. Willner, J. Phys. Chem. A 105 (2001) 3466.
[35] M.J. Hopper, J.W. Russell, J. Overend, J. Chem. Phys. 48 (1968) 3765.
[36] D.E. Milligan, M.E. Jacox, A.M. Bass, J.J. Comeford, D.E. Mann, J. Chem. Phys. 42 (1965) 3187.
[37] G.A. Carlson, G.C. Pimentel, J. Chem. Phys. 44 (1966) 4053.
[38] D.E. Milligan, M.E. Jacox, J.J. Comeford, J. Chem. Phys. 44 (1966) 4058.